InSAR Coherence–Decomposition Analysis

3 authors, including:

Some of the authors of this publication are also working on these related projects:

Project   METEWAVE - European Space Agency - ESTEC-21207/07/NL/HE View project

Project   Synergistic Use of SAR Constellations' Data Exploitation for Earth Science and Natural Hazard Response View project

InSAR Coherence Decomposition Analysis

Teng Wang, Mingsheng Liao and Daniele Perissin

Abstract—The phase coherence in Synthetic Aperture Radar Interferometry (InSAR) is often used in classification algorithms to detect possible temporal changes of the imaged terrain. However, in mountain areas the interferometric coherence is also sensitive to the slight variations of the acquisition geometry. In this letter we propose a very simple but effective method to separate the temporal decorrelation from the geometrical one. Assuming the imaged terrain can be modelled as a distributed target, the geometrical coherence can be estimated by exploiting a topographic model and the sensor acquisition parameters. The discrepancy between the geometrical coherence and the observed one can then be ascribed to temporal changes. Moreover, in presence of point-like targets, the hypothesis of distributed terrain is not valid any more and higher values of the observed coherence with respect to the synthetic geometrical one can be used to detect such targets. The proposed approach allows then in mountain areas 1) a simple and very fast rough estimation of the temporal coherence 2) the identification of point-like targets using just two images. The method has been applied and tested in the Badong (China) site using ERS tandem data.

Index Terms— coherence estimation, Synthetic Aperture Radar (SAR) interferometry

I. INTRODUCTION

COHERENCE is a measure of similarity of Interferometric Synthetic Aperture Radar (InSAR) echoes [1]. The magnitude of coherence is often used to describe different degrees of terrain changes. For example, bodies of water always show very low coherence; distributed targets such as agricultural fields show moderate coherence after one day, and low coherence after one month; rocks and artificial buildings in urban areas show high coherence even after years. Therefore, coherence plays an important role in certain InSAR applications, such as classification, change detection etc. [2]-[4].

Coherence between two complex signal s_1 and s_2 is defined as their correlation coefficient [1]:

$$\gamma = \frac{E\{s_1 \cdot s_2^*\}}{\sqrt{E\{|s_1|^2\} \cdot E\{|s_2|^2\}}} \qquad (1)$$

where s_1 and s_2 are complex signals from co-registered interferometric SAR images, $*$ is complex conjugate operator, $E\{\cdot\}$ means mathematical expectation.

Since mathematical expectation of radar signals is not attainable in practice, under the assumption of distributed targets, coherence is usually estimated by spatially averaging the radar echoes in a moving window [5]:

$$\hat{\gamma} = \frac{\sum_{i=1}^{L} s_{1i} s_{2i}^* \cdot e^{j\phi(i)}}{\sqrt{\sum_{i=1}^{L} |s_{1i}|^2} \sqrt{\sum_{i=1}^{L} |s_{2i}|^2}} \qquad (2)$$

where i denotes ith pixel in a Coherence Estimate Window (CEW). For each CEW, L pixels are used to obtain a coherence estimate.

As stated with more details in [6], there exist both under- and overestimate in the observed coherence map. The coherence estimates will bias to lower values because the correlated part of the signals contains interferometric fringes. Therefore, $\phi(i)$ that represent the topographic phase of ith pixel has to be compensated by means of Digital Elevation Model (DEM). Nevertheless, there also exist an overestimate bias that is due to the limited number of pixels in a CEW [5]. This bias becomes remarkable in low coherence areas. As a consequence, even incoherent signals rarely show zero coherence.

Moreover, coherence estimation is under the assumption of distributed targets. For a point-like target that dominates the reflected signal in a resolution cell, this assumption can not be valid. In order to correctly interpret the observed coherence map, different decorrelation sources and the extensions of targets have to be considered.

The observed coherence depends not only on target properties but also on geometric relations between the two acquisitions. Zebker and Villasenor modelled different decorrelation sources as [7]:

$$\gamma_{total} = \gamma_{temporal} \cdot \gamma_{geometric} \cdot \gamma_{thermal} \qquad (3)$$

where $\gamma_{thermal}$ depends on radar thermal noise, $\gamma_{temporal}$ measures the degree of physical changes of the illuminated surface over the period between acquisitions, $\gamma_{geometric}$ depends on the geometric relations between the two acquisitions[1].

For distributed targets, $\gamma_{geometric}$ can be measured from the ratio between overlapping and total spectra widths in the two dimensions of SAR image. In azimuth dimension, non-overlapping spectrum is caused by squint angle variation between the two images; in range dimension, it depends on normal baseline of the two acquisitions and terrain local slope [8].

For point-like targets, the relations between $\gamma_{geometric}$ and the physical extension of targets are described in [9]. In synthesis, higher coherence can be observed when the

Teng Wang and Mingsheng Liao are with the State Key Laboratory for Information Engineering in Surveying, Mapping and Remote Sensing, Wuhan University, Wuhan 430079, China (e-mail: wang.teng@gmail.com; liao@whu.edu.cn). Teng Wang and Daniele Perssin are with Dipartimento di Elettronica e Informazione, Politecnico di Milano, 20133 Milano, Italy (e-mail: daniele.perissin@polimi.it).

[1]In [7], the term $\gamma_{spatial}$ was used, however, in order to avoid confusion with the term "spatially average", we use $\gamma_{geometric}$ in the following discussions
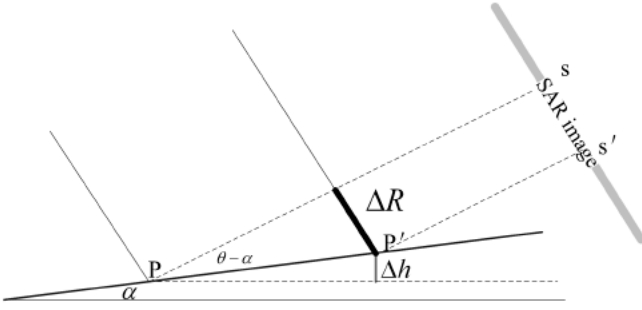
Fig. 1. Local slope geometry of SAR image. s and s' are two adjacent pixels in slant range axis. ΔR is their slant range difference, Δh is their elevation difference, θ is local incidence angle, α is the local slope of terrain.

target extension is smaller than the SAR resolution cell. This phenomenon offers a clue for locating point-like targets from only one interferogram.

Usually, azimuth and range spectral shift filtering are used to reduce the degree of interferogram noise by filtering out the non-overlapping part of spectra [8]. However, obtaining a better interferogram is not essential for applications such as change detection and/or classification. In this letter, instead of filtering, a simple but effective approach is proposed to decompose the observed coherence map. Firstly, $\gamma_{geometric}$ is estimated from geometric relations between the two acquisitions and an external DEM under distributed target assumption. Then the observed coherence is decomposed according to model (3). Since the thermal contributions caused by radar system noise are usually negligible [7], an appropriate temporal coherence map can be extracted. Moreover, given a stable point-like target, according to the relations between the target extension and the observed coherence, $\gamma_{geometric}$ estimated with distributed targets statistic will be lower than the observed value . If we consider the multiplicative model (3), possible point-like targets can be identified from the larger-than-one values in the extracted temporal coherence map.

II. COHERENCE DECOMPOSITION

A. Geometric Coherence Estimation

As presented in [8], for distributed targets, the geometric coherence between two SAR images can be estimated from the ratio between the overlapping spectra and bandwidths. In azimuth dimension, the non-overlapping spectrum can be obtained by calculating the Doppler frequency difference Δf_a. In range dimension, it can be obtained from the wavenumber shift Δf_r that has been described as [8]:

$$\Delta f_r = -\frac{c}{\lambda} \frac{B_n}{r \tan(\theta - \alpha)} \qquad (4)$$

where c is light velocity, λ is the wavelength of SAR signal, B_n is normal baseline, r is sensor-target distance, θ is incidence angle and α is local terrain slope. All the parameters in (4) can be obtained directly except α.

Let us assume a piece of distributed scattering terrain lying on a slope α with respect to the ground as described in Fig. 1. Two adjacent pixels s and s' in slant range axis are considered. They are collecting the contributions coming from the terrain

around P and P' with height difference Δh. The length $|PP'|$ can be written as:

$$|PP'| = \frac{\Delta R}{\sin(\theta - \alpha)} \qquad (5)$$

where θ and α have the same meaning as in (4), ΔR is the slant range difference. Since the elevation for each pixel can be obtained from the external DEM, Δh in Fig. 1 is known. Then, local slope α can be expressed as:

$$\sin(\alpha) = \frac{\Delta h}{|PP'|} \qquad (6)$$

Then, α can be written as:

$$\alpha = \arctan(\frac{\sin(\theta)}{\Delta R/\Delta h + \cos(\theta)}) \qquad (7)$$

With known α in (4), $\gamma_{geometric}$ can be derived from the ratio between the overlapping spectra and the bandwidths in range B_r and in azimuth B_a dimensions:

$$\gamma_{geometric} = \frac{B_a - |\Delta f_a|}{B_a} \cdot \frac{B_r - |\Delta f_r|}{B_r} \qquad (8)$$

In order to guarantee the validation of the $\gamma_{geometric}$ estimation, the accuracy of the external DEM has to be considered. From (4)-(8), the differential coefficients that represent the relations between Δh error and the consequently $\gamma_{geometric}$ error can be obtained as follows:

$$\frac{d\gamma_{geometric}}{d\alpha} = \frac{B_a - |\Delta f_a|}{B_a} \cdot \frac{cB_n}{B_r \lambda r \sin^2(\theta - \alpha)} \qquad (9)$$

$$\frac{d\alpha}{d\Delta h} = \frac{\Delta R \sin(\theta)}{\Delta R^2 + 2\Delta h \Delta R \cos(\theta) + \Delta h^2} \qquad (10)$$

where Δh can be also derived from α with (7). Therefore, for an interferometric system, given a tolerable $d\gamma_{geometric}$, the acceptable $d\Delta h$ is a function of the local slope α. A quantitative analysis that depends on the SAR system and the external DEM will be given in the next section.

B. Temporal Coherence Estimation

After estimating $\gamma_{geometric}$, $\gamma_{temporal}$ can be obtained by simply dividing the observed coherence map by $\gamma_{geometric}$. However, three particular points have to be considered: 1) overestimating bias; 2) point-like targets; and 3) volumetric decorrelation.

As previous analysis, depending on the local slope, the geometric coherence can even become close to zero. However, such values can not be obtained from the observed coherence estimation because of the overestimating biases. This phenomenon has to be taken into account in order to avoid meaningless outcomes when dividing the observed coherence by the geometric one . Thus, we flag the areas where the geometric coherence is less then a certain threshold. This allows also highlighting where low observed coherence is due to geometric decorrelation and not other reasons.

In high coherence areas, since geometric coherence is related to the extension of the targets [9], when a point-like scatterer dominates the reflected radar signal, the estimated

geometric coherence $\gamma_{geometric}$ may be smaller than the observed value. If so, the extracted temporal coherence will be larger than 1. Obviously, the temporal coherence should also be high enough to get such result; however, point-like targets usually have stable physical characteristic, which makes our assumption feasible.

It has to be mentioned that, in order to keep the procedures of our approach as simple as possible, volumetric coherence is ignored in the decomposition model. Nevertheless, since no volumetric decorrelation can be expected from the point-like targets, this ignorance do not influence our target detection result. On the other hand, because the value of volumetric coherence represents the elevation variance within a resolution cell [8], different densities of vegetation can be observed from the decomposed coherence map. As future work, if multi coherence maps are available, volumetric coherence can be considered in the coherence decomposition model. Then, it is also possible to quantitatively analyze the different densities of vegetations from the extracted volumetric coherence map.

III. RESULTS

The Results presented in this letter are obtained with ERS-1/2 Tandem data acquired in January, 1996. The normal baseline is 199m. The test site is around Badong county, Three Gorges area, China. The CEW used here is 15 pixels in azimuth and 3 pixels in range.

Fig. 2 shows the observed coherence map of our test site, the topographic phase has been removed by means of Shuttle Radar Topography Mission (SRTM) DEM. The resolution of SRTM DEM is $90\,$m, lower than the one of ERS SAR image (about $5\,$m in azimuth and $25\,$m in range). A simulated SAR image was generated from the SRTM DEM and then co-registered to the master image to obtain an elevation map in SAR coordinates. Although the resolution and accuracy of SRTM DEM are not high, they are sufficient for compensating the interferometric fringes during coherence estimation [3]. From Fig. 2, the Yangtze River can be recognized in the middle. However, the river boundaries are not so clear, especially in the right part. Below Yangtze River, many areas with low coherence can be seen. Without *a priori* information, it is difficult to detect different temporal coherence levels.

Different from $\gamma_{observed}$ estimation, the accuracy of SRTM DEM has to be evaluated for estimating $\gamma_{geometric}$. Given the parameters of the ERS data set: $B_r = 16\,\text{MHz}$, $\lambda = 5.66\,\text{cm}$, $r = 847\,\text{km}$, $\theta = 23^\circ$, $Bn = 199\,\text{m}$ and $\frac{B_a - |\Delta f_a|}{B_a} = 0.8$, and given maximum tolerable error $d\gamma_{geometric} = 0.1$, the acceptable $d\Delta h$ values can be obtained from (9) and (10) and shown as a function of the local slope α in Fig. 3.

From Fig.3, the highest requested Δh accuracy (about 5m) is needed only when the local slope is near 90° (in radar shadow areas, i.e. $\alpha < -67^\circ$, high accuracy DEM is also needed, however no coherent information could be expected from such areas). For most terrain slopes, say from -10° to 10°, $10\,\text{m}$ Δh accuracy is enough for obtaining a geometric coherence estimate with $d\gamma_{geometric} < 0.1$. Moreover, since the simulated SAR elevation map has to be interpolated from sparser SRTM DEM grids, SRTM DEM error can be strongly
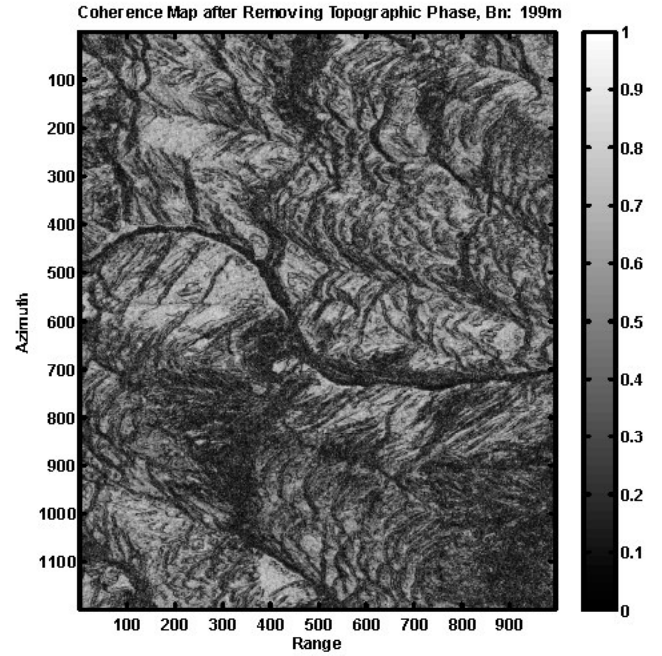

Fig. 2. Observed coherence map of Badong test site, for coherence estimating, the topographic phase has been removed with SRTM DEM.

reduced by calculating the height difference Δh between two adjacent pixels in SAR coordinates. In other words, because of the differential operation, both low and high pass SRTM DEM errors are partially cancelled out. As a consequence, a higher accuracy can be expected from Δh estimate. To sum up, in our approach, $10\,\text{m}$ accuracy SRTM DEM is enough for obtaining a $\gamma_{geometric}$ estimate whose error is less than 0.1. The resultant geometric coherence map is shown in Fig. 4. It is easy to realize that the geometric coherence is strongly related to the terrain in this test site. In some areas, very low coherence can be observed.

After coherence decomposition analysis, the extracted temporal coherence map is shown in Fig. 5. The areas with geometric coherence lower than 0.2 are flagged as zero in order to distinguish them from low temporal coherence areas. In Fig 6. the histograms of $\gamma_{geometric}$, $\gamma_{observed}$ and $\gamma_{temporal}$ are plotted together, from which the proposed approach shows the capability of temporal coherence extraction. Because of the one-day temporal baseline, most of the pixels show high temporal coherence after the coherence decomposition.

Compared with Fig. 2, the vegetated areas show moderate coherence in Fig. 5 instead of low values. Even different densities of vegetation can be recognized without the affection of topography. The resultant temporal coherence map is helpful for correctly interpreting different types of surfaces. For qualitatively assessing our result, the observed and extracted temporal coherence along the Yangtze River are geocoded and shown with the optical image from Google Earth in Fig. 7. It has to be noticed that the river is narrower in the coherence maps than in the optical image because the SAR images were acquired before the construction of the Three Gorges Dam. A significant example to be shown is pointed out with arrows in
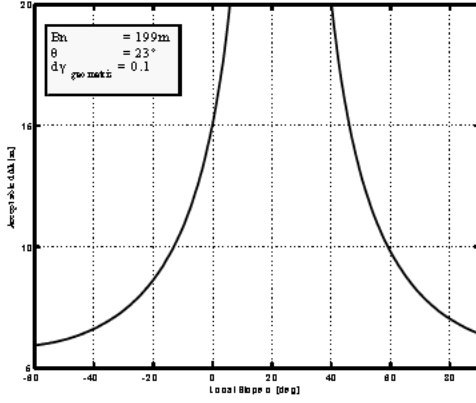
Fig. 3. Given $d\gamma_{geometric} = 0.1$, acceptable $d\Delta h$ from the external DEM is plotted as a function of the local slope α.
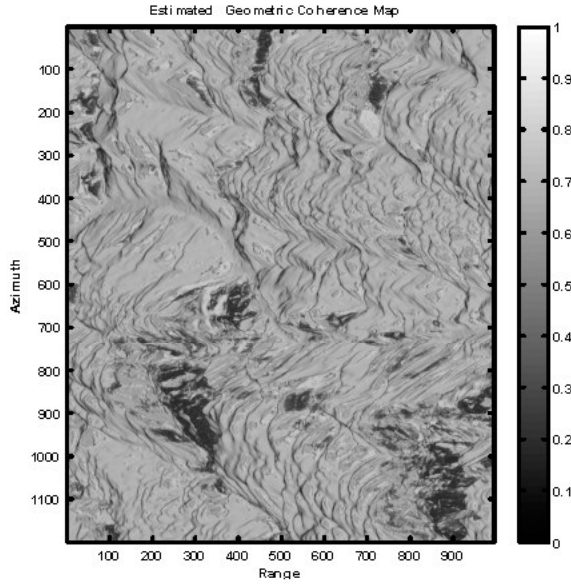

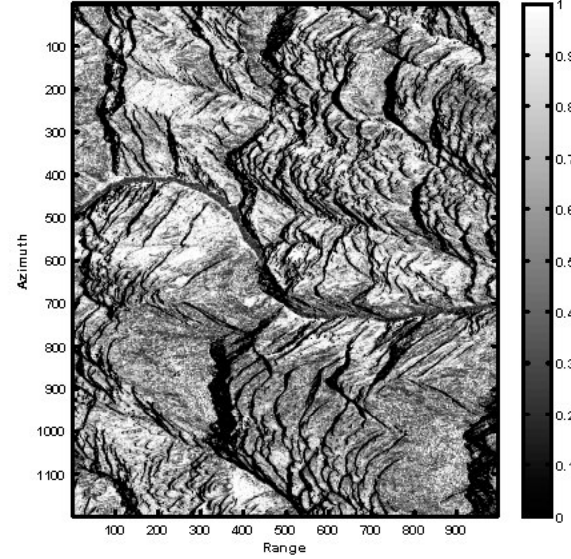Fig. 4. Estimated geometric coherence map of Badong test site.

Fig. 5. Extracted temporal coherence map from coherence decomposition analysis.
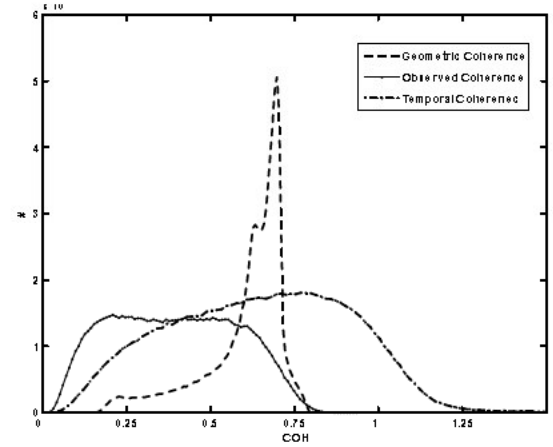
Fig. 6. Histogram of the observed coherence and the estimated geometric and temporal coherence.

Fig. 7, it is easy to distinguish the radar shadow and vegetation areas from our result.

The east part of the riverbank shows high coherence in both Fig. 7 (a) and (b). As discussed in Section I, larger-than-one "coherence" can be obtained when the distributed target hypothesis is not valid. A typical area with this kind of targets is indicated within the black rectangle in Fig. 7 (b) and the details are shown in Fig. 8. For better understanding the locations of point-like scatterers, larger-than-one pixels are plotted with the values scaled from 1 to 1.2. For evaluating the locations of the detected stable point-like targets, Permanent Scatterer (PS) InSAR analysis [10] was carried out in this test site with 12 ERS SAR images. The PSs with temporal coherence higher than 0.95 are shown in red cross in Fig. 8.

Because of the short spatial and temporal baselines of our tandem images, the number of possible point-like scatterers detected from our approach is obviously more than the number of PSs. Moreover, since observed coherence is estimated from

moving CEWs, locally maximum coherence surrounded by reducing values can be observed from the enlarged view in Fig. 8. It could be difficult to precisely locate the position of point-like targets from the low resolution coherence map. Nevertheless, from Fig. 8 most of the possible PSs were identified from the coherence decomposition analysis (6 misdetections in 93 PSs). The 6.5% misdetection rate can be explained by the $\gamma_{geometric}$ estimation errors. We could set the threshold slightly less than 1, say 0.98, then all PSs can be detected by our approach. In the worst case, the result can be used as point-like scatterer candidates in many target detection algorithms. Our future work is going to be estimating the locations and extensions of point-like scatterers from multi coherence maps.

IV. CONCLUSIONS

In this letter, a simple approach to decompose observed InSAR coherence map was presented. Instead of filtering,

Fig. 8. Details in the area indicated within the black rectangle in Fig. 7 (b). Point-like targets show larger-than-one values after the coherence decomposition. The pixels with resultant "coherence" from 1 to 1.2 are shown with the point-like scatterers detected by Permanent Scatterer InSAR analysis (red cross).
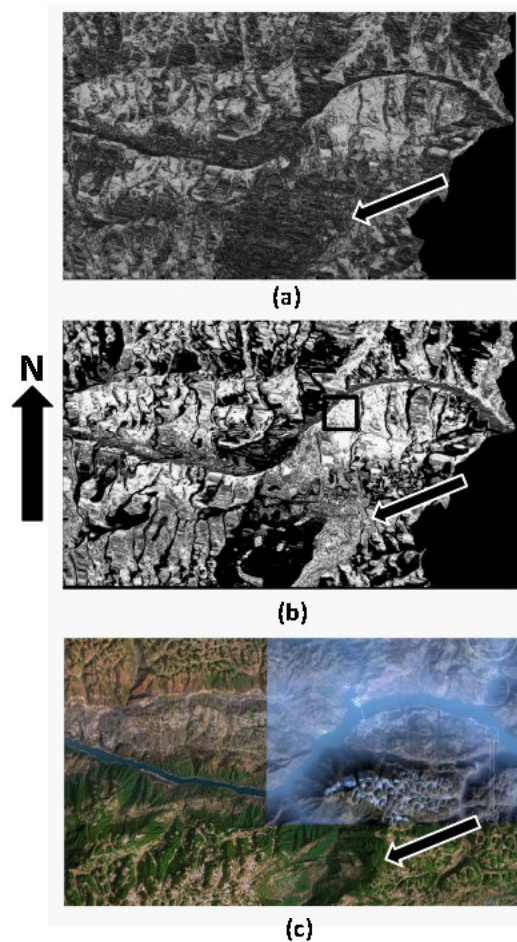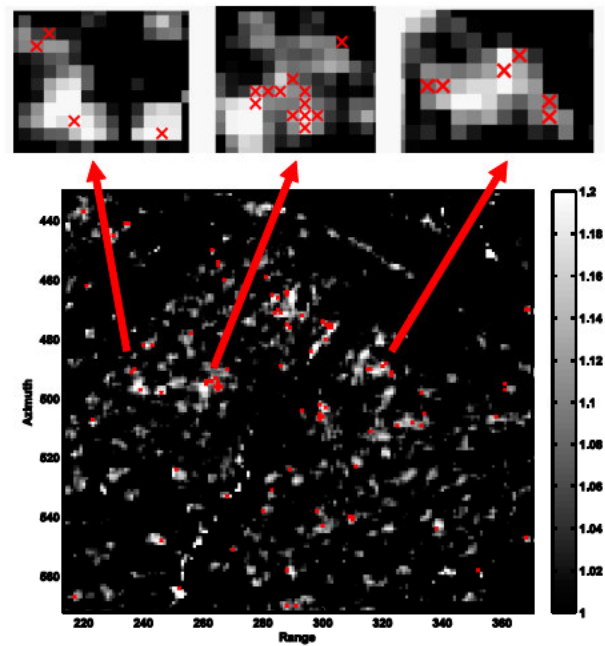

Fig. 7. One part of our test site that is along Yangtze River. (a): geocoded observed coherence map, (b): geocoded extracted temporal coherence map, (c): optical image from Google Earth. The arrows in (a) and (b) point at an area with steep terrain and vegetation. The black rectangle in (b) indicates a typical area with possible point-like targets, where the details are shown in Fig. 8.

we separated the estimated geometric coherence from the observed one for obtaining an approximately temporal coherence map. The geometric coherence was estimated from sensor parameters and SRTM DEM. Since the geometric coherence estimation is performed with distributed target statistic, for stable point-like targets, the estimated coherence is lower than the observed values. As a consequence, larger-than-one values can be used to identify the possible stable point-like target from only one interferogram. The results in Three Gorges area qualitatively demonstrated the improvement of the extracted temporal coherence and the locations of point-like targets. Although the temporal coherence map and point-like targets locations are estimated in an approximate way, the simple and fast procedures make the approach be useful for many coherence based applications.

V. ACKNOWLEDGMENT

REFERENCES

[1] S. H. C. L. Werner, and P. Rosen, "Application of the interferometric correlation coefficient for measurement of surface change," presented at AGU Fall Meeting, San Francisco, CA, 1996.

[2] P. A. Rosen, S. Hensley, I. R. Joughin, F. K. Li, S. N. Madsen, E. Rodriguez, and R. M. Goldstein, "Synthetic aperture radar interferometry," *Proceedings of the IEEE*, vol. 88, pp. 333-382, 2000.

[3] M. Santoro, J. I. H. Askne, U. Wegmuller, and C. L. Werner, "Observations, Modeling, and Applications of ERS-ENVISAT Coherence Over Land Surfaces," *Geoscience and Remote Sensing, IEEE Transactions on*, vol. 45, pp. 2600-2611, 2007

[4] J. I. H. Askne, P. B. G. Dammert, L. M. H. Ulander, and G. Smith, "C-band repeat-pass interferometric SAR observations of the forest," *Geoscience and Remote Sensing, IEEE Transactions on*, vol. 35, pp. 25-35, 1997.

[5] R. Touzi, A. Lopes, J. Bruniquel, and P. W. Vachon, "Coherence estimation for SAR imagery," *Geoscience and Remote Sensing, IEEE Transactions on*, vol. 37, pp. 135-149, 1999.

[6] H. A. Zebker and K. Chen, "Accurate estimation of correlation in InSAR observations," *Geoscience and Remote Sensing Letters, IEEE*, vol. 2, pp. 124-127, 2005.

[7] H. A. Zebker and J. Villasenor, "Decorrelation in interferometric radar echoes," *Geoscience and Remote Sensing, IEEE Transactions on*, vol. 30, pp. 950-959, 1992.

[8] F. Gatelli, A. M. Guamieri, F. Parizzi, P. Pasquali, C. Prati, and F. Rocca, "The wavenumber shift in SAR inferometry," *Geoscience and Remote Sensing, IEEE Transactions on*, vol. 32, pp. 855-865, 1994.

[9] D. Perissin, C. Prati, M. E. Engdahl, and Y. L. Desnos, "Validating the SAR Wavenumber Shift Principle With the ERS Envisat PS Coherent Combination," *Geoscience and Remote Sensing, IEEE Transactions on*, vol. 44, pp. 2343-2351, 2006.

[10] A. Ferretti, C. Prati, F. Rocca, "Permanent scatterers in SAR interferometry", *Geoscience and Remote Sensing, IEEE Transactions on*, vol. 39, no. 1, 2001